APPLICATION OF NON-NEGATIVE SPARSE MATRIX TRANSFORMATION IN HYPERSPECTRAL ANALYSIS**

Z. Deng, Y. Fu*, S. Zhao, Y. Gao, J. Cui

Changchun University of Science and Technology, School of Optoelectronic Engineering, Changchun, China; e-mail: linda_fy@cust.edu.cn

A variety of pictures in hyperspectral fields requires a reduction in dimensionality, which often needs unique algorithms such as principal component analysis and minimum noise fraction (MNF). This article investigates the improved method of non-negative sparse matrix transformation based on the maximum likelihood covariance estimation and the Frobenius norm to better achieve dimensionality reduction. Non-negativity is presented based on the sparse matrix, which reduces the calculation time and improves efficiency. In order to verify the non-negative sparse matrix transforms (n-SMT) algorithm, samples eroded by disease were selected in the experiment and classified to identify the different parts of leaves after dimension reduction. Besides the n-SMT method, the MNF algorithm is also applied to all the samples. This article compares the two algorithms' operating time and verifies the accuracy of classification after the n-SMT algorithm.

Keywords: *non-negative sparse matrix, matrix transformation, hyperspectral image, image processing.*

ПРИМЕНЕНИЕ ПРЕОБРАЗОВАНИЯ НЕОТРИЦАТЕЛЬНОЙ РАЗРЕЖЕННОЙ МАТРИЦЫ ПРИ ГИПЕРСПЕКТРАЛЬНОМ АНАЛИЗЕ

Z. Deng, Y. Fu*, S. Zhao, Y. Gao, J. Cui

УДК 535.3;535.317.1

Чанчуньский университет науки и технологий, Чанчунь, Китай; e-mail: linda_fy@cust.edu.cn

(Поступила 15 июня 2021)

Для снижения размерности при обработке гиперспектральных изображений предложен усовершенствованный метод преобразования неотрицательной разреженной матрицы (n-SMT), основанный на оценке ковариации максимального правдоподобия и норме Фробениуса. Неотрицательность разреженной матрицы сокращает время расчета и повышает эффективность. Для проверки алгоритма n-SMT образцы листьев элеутерококка колючего, пораженных заболеванием, классифицированы для идентификации различных частей листьев после уменьшения размерности. Наряду с n-SMT для всех образцов применен алгоритм вычисления минимальной доли шума. Сравнивается время работы двух алгоритмов и проверяется точность классификации с помощью алгоритма n-SMT.

Ключевые слова: *неотрицательная разреженная матрица, матричное преобразование, гиперспектральное изображение, обработка изображений.*

Introduction. Hyperspectral imaging analysis [1–4], combining imaging and spectral technologies, has multitudinous applications in remote sensing detection and many other fields owing to its extremely high resolution and certain spectral information. More specifically, the third dimension of hyperspectral imaging has much more data than traditional spectra and will cause severe problems in computing. There is a great need to reduce dimension before data processing [5]. Lots of methods and algorithms are widely used in dimensionality reduction. Principal components analysis (PCA) is considered the most widespread and com-

**Full text is published in JAS V. 89, No. 3 (http://springer.com/journal/10812) and in electronic version of ZhPS V. 89, No. 3 (http://www.elibrary.ru/title_about.asp?id=7318; sales@elibrary.ru).

mon algorithm in the dimensionality reduction field, using the covariance matrix to achieve the reduction of dimension. In addition, another widely applied algorithm is named the minimum noise fraction (MNF) rotation [6], which performs PCA transformations twice and separates the noise from the data. Generally, covariance estimation is required in the data dimensionality reduction stage of remote sensing data processing. Both of the algorithms mentioned above use this method, especially PCA, which requires accurate estimation of the covariance matrix.

However, in small target detection, the above two algorithms have limitations, which will be introduced in below. In that case, a new algorithm sparse matrix transform (SMT) was gradually realized for its superiority [7–9]. These SMT-based algorithms are inseparable from sparse matrices and are mainly used to decompose the covariance matrix [10, 11] as well as to simplify the data. In this paper, we also get inspiration from the MNF and introduce non-negative matrices [12–17]. In addition, we combine the positive matrices with the basic algorithm. The SMT has advantages of accuracy and efficiency compared with other methods typically used as a compressive technique. It also solves the problem of the signal-to-noise ratio and the influence of image value change. After the SMT algorithm is proposed, later generations also make improvements to this algorithm. For example, some researchers put forward sparse matrix transformation with shrinkage (s-SMT) [18]. Some researchers also indicate that if the sparse matrices are non-negative, they can increase the speed of dimensionality reduction and improve the classification results of hyperspectral data.

The method of non-negative SMT (n-SMT) is proposed to achieve dimensionality reduction. We compare it with other methods to illustrate the advantage of our improved algorithm. Finally, we add a support vector machine (SVM) [19–21] after reduction to complete the data processing and indicate that each algorithm has differences in operating time and steps. The evaluation index for the SVM classification is the receiver operating characteristic (ROC) curve [22, 23]. The critical area between the curve and the coordinate axis is considered an indicator of the quality of the classification. During the experiment, we choose *Acanthopanax senticosus* as a tiny sample detection target. Moreover, we explain the advantages of the SMT in dimensionality reduction by comparing the accuracy of different algorithms.

MNF algorithm. Minimum noise fraction (MNF) rotation is the method used in digital image processing. This algorithm proposes multi-dimensional (multi-band) orthogonal linear transformation based on statistical characteristics.

The key element for the MNF algorithm is the covariance matrix, so let us get the covariance matrix in the first step. It is necessary to use the high-pass filter template to filter the entire image or image data blocks for obtaining the noise covariance matrix C_N and diagonalizing it to get D_N:

$$D_N = U^T C_N U, \tag{1}$$

where D_N is a diagonal matrix with the eigenvalues of C_N arranged in descending order and U is an orthogonal matrix composed of eigenvectors. Making a further transformation, we can obtain:

$$I = P^T C_N P, \tag{2}$$

$$P = U D_N^{-1/2}, \tag{3}$$

where I is the identity matrix, P is the transformation of the sample data X, $Y = PX$. So, we project the original image into a new space. It should be noted that the noise in the resulting transformed data has unit variance, and it is uncorrelated between bands. The next step is as follows. We use P to transform the total variance matrix C_D of the image for obtaining the total covariance matrix $C_{D\text{-}adj}$ after adjusting for noise:

$$P^T C_D P = C_{D\text{-}adj}. \tag{4}$$

After processing the covariance matrix and obtaining the eigenvector matrix V, we can get the following formula:

$$C_{D\text{-}adj} V = D_{D\text{-}adj}, \tag{5}$$

where $D_{D\text{-}adj}$ is the diagonal matrix in which the eigenvalues corresponding to the eigenvector matrices V are arranged in descending order.

These are all steps of the MNF transformation. We can notice that it operates PCA twice and arranges the images in descending order according to the signal-to-noise ratio. The top ones contain most of the information, thus achieving data dimensionality reduction.

Add non-negative matrix on transformation. We will introduce a method in response to the overfitting questions raised above. Sparse matrix transformation based on maximum likelihood is the most commonly employed choice for estimating covariance from data.

Let us use x_n to represent the number of total samples and organize them in a data matrix $X = [x_1, x_2, \ldots, x_n]$. The dimension of each column vector x_i is p. Let us use the dimensional reduction operator E_q of $p \times q$ dimensions. The sample covariance S of the original data X is given by $S = (1/n)XX^T$. We take matrix R as the unbiased estimator of S, where R is given by $R = E(S)$. Let $R = E\Lambda E^T$, where Λ is the diagonal matrix of eigenvalues and E is the orthogonal matrix of eigenvectors.

For a vector X whose column is independent and has Gaussian distribution with a zero mean, we have for the likelihood of the x estimation:

$$p_R(X) = \frac{1}{(2\pi)^{np/2}}|R|^{-n/2}\exp\left\{-\frac{1}{2}\text{trace}\left\{X^T R^{-1} X\right\}\right\}. \quad (6)$$

In the case of $R = S$ we can regard the sample covariance as the true covariance of the maximum likelihood estimation. Then we can conclude

$$\text{trace}(X^T R^{-1} X) = n\ \text{trace}(R^{-1} S). \quad (7)$$

Thus, we can get

$$p_R(X) = \frac{1}{(2\pi)^{np/2}}|R|^{-n/2}\exp\left\{-\frac{1}{2}n\,\text{trace}\left\{R^{-1} S\right\}\right\}. \quad (8)$$

Taking the logarithm of the above formula, we can get $\ln X = (-n/2)\text{trace}\{\text{diag}(E^T SE)\Lambda^{-1}\}$,

$$-(n/2)\ln|\Lambda| - (np/2)\ln(2\pi). \quad (9)$$

Our purpose is to get the maximum likelihood estimation, so we need to use the following:

$$\hat{E} = \arg\min_{E\in\Omega}\left\{\left|\text{diag}(E^T SE)\right|\right\},$$

$$\hat{\Lambda} = \text{diag}(\hat{E}^T S\hat{E}). \quad (10)$$

Here, Ω is a set conforming to the orthogonal transformation. Then, $\hat{R} = \hat{E}^T\hat{\Lambda}\hat{E}$ is the maximum likelihood estimation of the covariance.

As the number of data samples are less than the number of bands, the sample covariance can overfit the data after these transformations. Compared with PCA and MNF transformation, these unique processes laid a good foundation for the following.

The key idea of the SMT is to restrict the vector Ω, so we set a model to effectively conduct the E matrix estimation. Each component of the matrix E should be orthonormal. Thus, matrix E can be rewritten with the help of a product of K sparse orthonormal matrices:

$$E = \prod_{k=1}^{K} E_k = G_1 G_2 \ldots G_K. \quad (11)$$

Each sparse matrix E_K is given by a form of $G = I + \Theta(i,j,\theta)$, where $\Theta(i,j,\theta)$ is fulfilled by the following conditions:

$$\Theta(i,j,\theta) = \begin{cases} \cos(\theta) - 1, & \text{if } r = s = i \text{ or } r = s = j, \\ \sin(\theta), & \text{if } r = i \text{ and } s = j, \\ -\sin(\theta), & \text{if } r = j \text{ and } s = i, \\ 0, & \text{otherwise.} \end{cases} \quad (12)$$

Different situations for the choice of the angle θ are illustrated in Fig. 1. We notice that each 2D rotation G_k plays a similar role for the fast Fourier transform (FFT) algorithm [24] (as "X"). However, for the FFT algorithm "X" has to follow certain periodicity laws, but for the SMT algorithm the procedure of "X" formation is not restricted by any adjacent vectors, which means that each "X" can have an arbitrary θ angle. The arrangement and distribution of "X" can be applied to various types of hyperspectral data. This makes the SMT model promising for data dimensionality reduction.

Using the SMT model constraint, the ML estimation of E is given by:

$$\hat{E} = \arg\min_{E=\Pi_{k=1}^{K} E_k}\left|\text{diag}(E^T SE)\right|. \quad (13)$$

k changes from 0 to $K - 1$, so, we have to determine the coordinates of the two points i_k and j_k:

$$\left(i_k, j_k \right) \leftarrow \arg\min_{(i,j)} \left(1 - \frac{\left[S_k \right]_{ij}^2}{\left[S_k \right]_{ii} \left[S_k \right]_{jj}} \right). \tag{14}$$

Each pair (i_k, j_k) determines the correlated function, and by solving the equation, we can get the angle θ_k

$$\theta_k = (1/2)\text{atan}\left(-2\left[S_k \right]_{i_k j_k}, \left[S_k \right]_{i_k i_k} \left[S_k \right]_{j_k j_k} \right). \tag{15}$$

Using the two formulas above, we can get the relationship between G and S_k, which can be expressed by the following matrix operation:

$$G^* = \arg\min(\text{diag}_G(G^T S G), \tag{16}$$

$$S_{k+1} = G^T S_k G. \tag{17}$$

In this way, we can get multiple sets of G^* through the iteration method; the product of each G is the matrix we want. By calculating the result of the continuous product, $\hat{E}$ (the ML estimate of E) can be found. The SMT process is represented below. Here we assume that the number of rotations is K. Using the matrix iteratively, we can get the result of the dimensionality reduction:

Input the sample covariance matrix S, get $F_{ij} = S_{ij}^2/(S_{ii}S_{jj})$
  $k = 1, \ldots, K$.
  Find the value of i,j that maximizes F_{ij}
  Find the angle of $\theta = (1/2)\text{atan}(-2S_{ij}, S_{ii} - S_{jj})$
  Find $G = I + \Theta(i,j,\theta)$
  Update $S = G^T S_k G$
  Get the feature matrix $E = G_1 G_2 \ldots G_k$
  Get the feature diagonal matrix $\Lambda = \text{diag}(S)$
  Take the first q maximum values of Λ to form $\Lambda_q = (i_1, \ldots, i_q\}$.

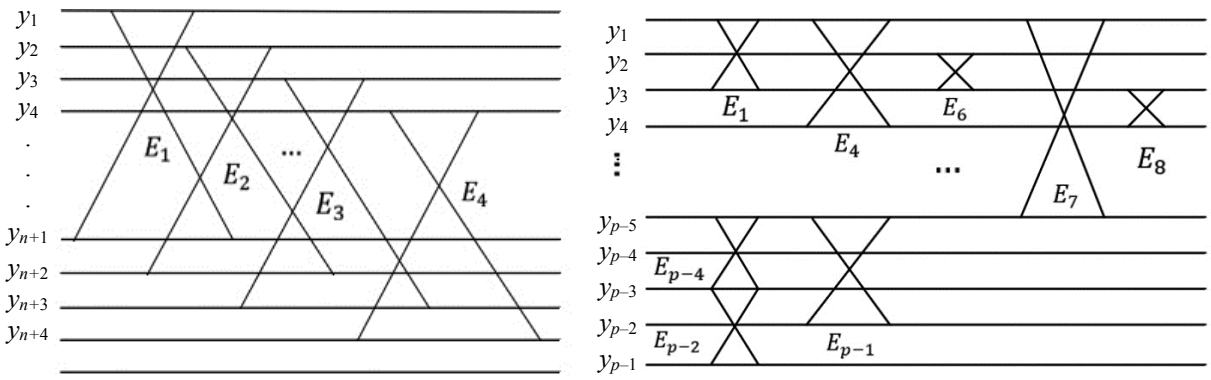

Fig. 1. Comparison between the fast Fourier transform and the SMT methods. The SMT is transformed by a variety of normalized orthogonal matrices. The cross multiplication is arbitrary.

Non-negativity of the sparse matrix. We assume that all the entries are positive in the calculating process of the SMT algorithm, which improves some of the limitations of the SMT without changing the algorithm logic and results. The samples cannot have negative characteristics. So, for this algorithm, during estimation of the covariance matrix, we suppose that negative entries are forbidden for elements of any matrices in their combination. This is for the following reason. If positive and negative matrices combine, the eigenvalue of the covariance would disappear; thus, we fail to reach the step of Givens rotations unless we set a limitation of the non-negativity. In this case, we need to introduce the non-negative sparse matrix.

However, in the matrix negative elements will inevitably appear during the process of calculation. Thus, the n-SMT algorithm must apply some linear transformations called 'rotations', in the jargon of the reduction algorithm. As for Eq. (11), we can redefine the adjacent matrix pairs when decomposing the matrix E while negative matrices appear. Let assume that G_i is the matrix we need to redefine, then the production of $G_i G_{i+1}$ can be rewritten in the form:

$$G_i G_{i+1} = G_i T T^{-1} G_{i+1}, \tag{18}$$

where the new rotated factors are $G_i^* = G_i T$ and $G_{i+1}^* = T^{-1} G_{i+1}$.

As for the additional matrices T and T^{-1}, we would introduce a kind of matrix pair:

$$T = \begin{vmatrix} 1 & 0 & \dots & 0 & 0 \\ 0 & 1 & \dots & a & 0 \\ \dots & \dots & \dots & \dots & \dots \\ 0 & 0 & \dots & 1 & 0 \\ 0 & 0 & \dots & 0 & 1 \end{vmatrix}, \quad T^{-1} = \begin{vmatrix} 1 & 0 & \dots & 0 & 0 \\ 0 & 1 & \dots & -a & 0 \\ \dots & \dots & \dots & \dots & \dots \\ 0 & 0 & \dots & 1 & 0 \\ 0 & 0 & \dots & 0 & 1 \end{vmatrix} \tag{19}$$

It is worth noting that the matrix pair needs to be multiplied by the same factor a.

The above matrix transformation process clarified the non-negativity of sparse matrices, directly related to the generation of sparse matrices. When processing the production of a series of sparse matrices, compared with MNF, no subtraction can occur because of the non-negativity entries in the matrices, which satisfies our requirements for sparse matrices very well.

Experiments. We chose *Acanthopanax senticosus* as the sample of the experiment, irradiated by a hyperspectral instrument. All the samples used were obtained from the Institute of Economic Botany, Changchun Academy of Agricultural Sciences, Jilin Province. With the cooperation of the researchers of the Institute, we selected the diseased plants and determine the effected locations, so as to verify the experimental result at the end.

As for the instruments, we have selected a complete hyperspectral detection system. The whole system comprises four parts, including a scanning spectrometer, a CCD camera, a halogen lamp linear light source, and a one-dimensional translation stage. The entire system is encapsulated in a dark box to avoid interference from ambient light. Hence, before the data acquisition, the optical imaging system needs to be adjusted, and the control parameters of the stage must be set.

Hyperspectral data dimensionality reduction methods can be roughly divided into two categories. In this article, we first remove the useless brands, which include noise, and streaks with obvious errors. As for the spectral preprocessing technology, the standard deviation of each band can reflect the spectral discrimination. Hence, we can use the statistical information to eliminate interference in the dataset. We notice that the standard deviation of the 1000- to 1350-nm wavelengths is higher than the value of the 1500-nm wavelength. A band with a significant standard deviation means that the correlation with other bands can be ignored so that this band interval can be selected as a characteristic band. At the same time, these bands contain lots of sub-information.

Figure 2 also reveals the average value of the spectral data of each band. The curves between average value and another wavelength are roughly the same shape. This result confirms the rationality of our choice of sensitive wavelength bands. After determining the characteristics of the wavelength, we perform false-color synthesis of the hyperspectral data. This process is a further certification of the premise of our dimensionality reduction. In this experiment, the light source functions used the near-infrared band (900–1700 nm). Even though the information contained in the image can still maintain a comprehensive wealth of information after false-color synthesis, we select a band with a more significant standard deviation within different bands. Also, we consider the correlation between the adjacent bands of the hyperspectral image, which is

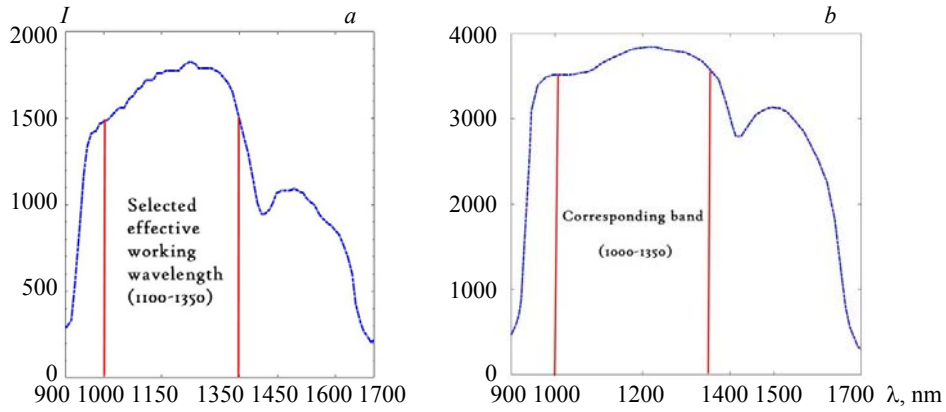

Fig. 2. The standard deviation (a) and mean value (b) of each wavelength. I represents the pixel intensity of the image at each wavelength.

higher than for the far bands. Finally, we selected two bands (1000–1350, 1450–1500 nm) to synthesize the color image. Figure 3 shows the effect of false-color synthesis. The three different color spectrum curves represent three different states of the sample: red color corresponds to leaves, yellow color to disease, and blue color to the background. The spectral curve has obvious changes within the range 1100–1300 nm; thus, the SMT algorithm is feasible after preprocessing.

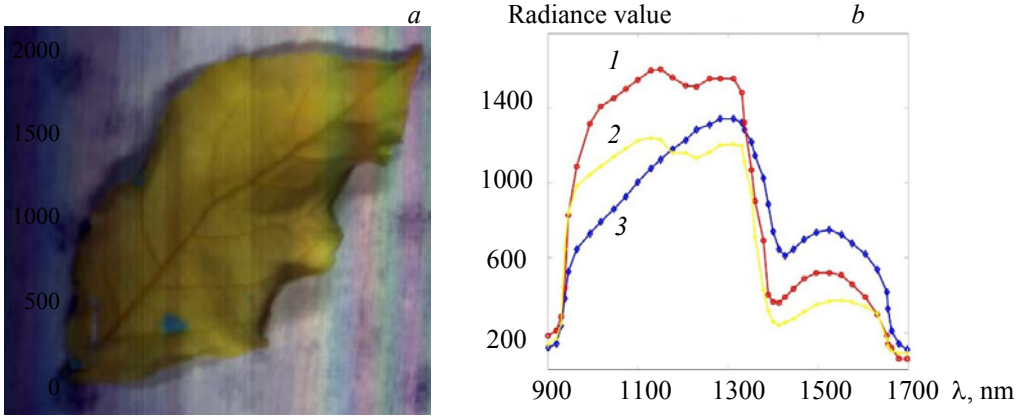

Fig. 3. (a) False-color synthesis of a diseased leaf and (b) the corresponding spectral curve: 1 – corresponds to leaves, 2 – to decrease, and 3 – to the background.

After preprocessing, the figure is fully prepared for the algorithm. The next step is to apply the n-SMT to the image. First, the n-SMT covariance estimation is used to determine the covariance matrix for the image. The n-SMT estimation can produce a complete set of eigenvalues from a limited number of images in MATLAB software. All the elements in the matrices are positive. It is worth noting that the requirements of the n-SMT algorithm for noise are different than those of other algorithms; hence, we pay more attention to the treatment of noise. It should be noted that the noise had been removed in the previous section.

Figure 4 shows the result of n-SMT and sorts the first six eigen-leaves. According to our analysis, the first six bands contain most of the information (about 87%) of the image. The contribution of the rest bands is shown in Fig. 5. We can find a dark spot in Fig. 4d differing from other parts in the picture. At the same time, in Fig. 4b, the blade part is marked with highlights for greater visibility of the leaves' outline. These phenomena indicate that the reduced dimensionality of the independent image can characterize some features of the original image, which brings convenience for subsequent classification and image analysis.

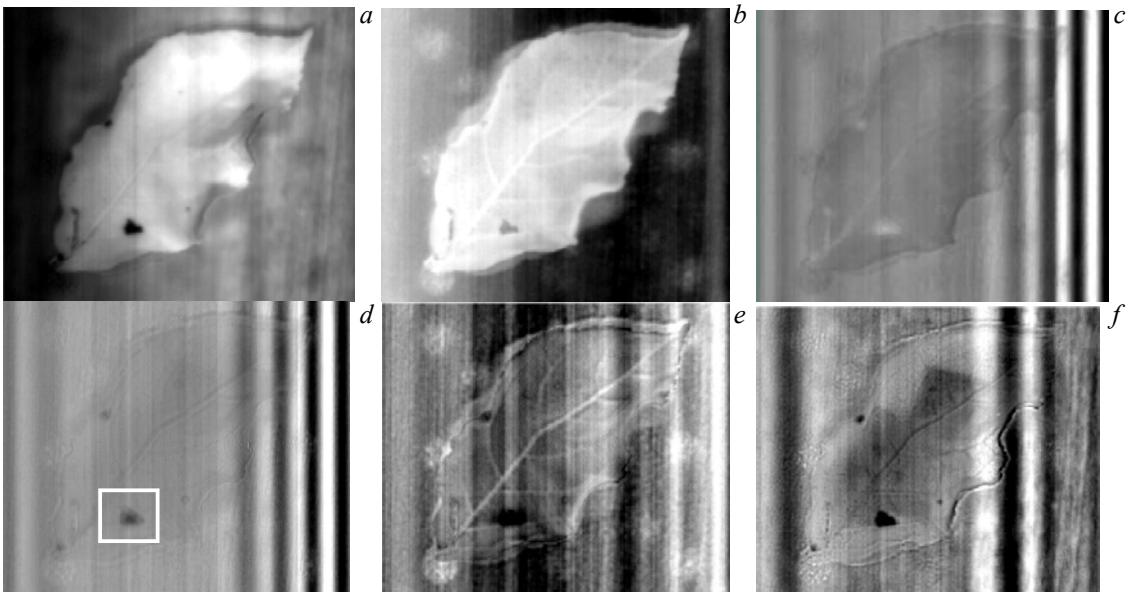

Fig. 4. Result of applying the sparse matrix transform and sorting by component contribution.

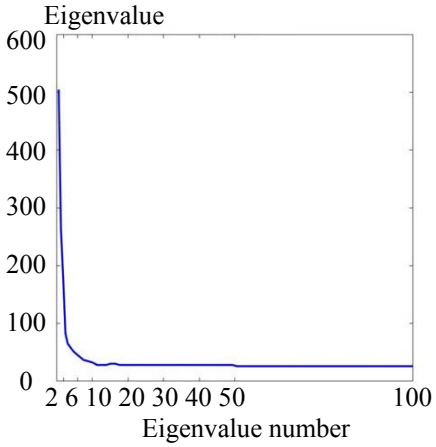

Fig. 5. The eigenvalue line graph of the transformed band and the cumulative variance of the first six characteristic leaf images.

It is worth noting that the n-SMT algorithm has advantages with regard to computing speed and accuracy. We first illustrated the time superiority. For comparison, we used the MNF algorithm. The results of comparing the operating time between two algorithms are represented in Table 1. The time domain superiority of the SMT is 2.86 s of operating time, nearly 7 s faster than the MNF (9.55 s of operating time) in computing speed. We processed only one picture in this experiment. However, in multi-sample data processing, with a large sample dataset, each sample has multiple dimensions. The advantages of the SMT computing speed will bring greater convenience.

After the dimensionality reduction process, we apply the SVM classifier to illustrate the effectiveness and feasibility of the n-SMT method. In this experiment, we use four different kernel functions to classify the reduction result of the images. It can be seen that after four times processing of the SVM classifier, the difference between the kernel function is inconspicuous. The differences reflect that the n-SMT algorithm preserves the information of the original data well. Figure 6 shows the result of classification and is mainly composed of three colors: red, blue, and green, corresponding to the disease, leaves, and background respectively. In general, the four types of results show no difference when using the SVM; only some tiny differences exist in a part that is shown as a white square area. There is also a detailed difference in the sample boundary area, which is caused by the different parameter settings within each kernel function.

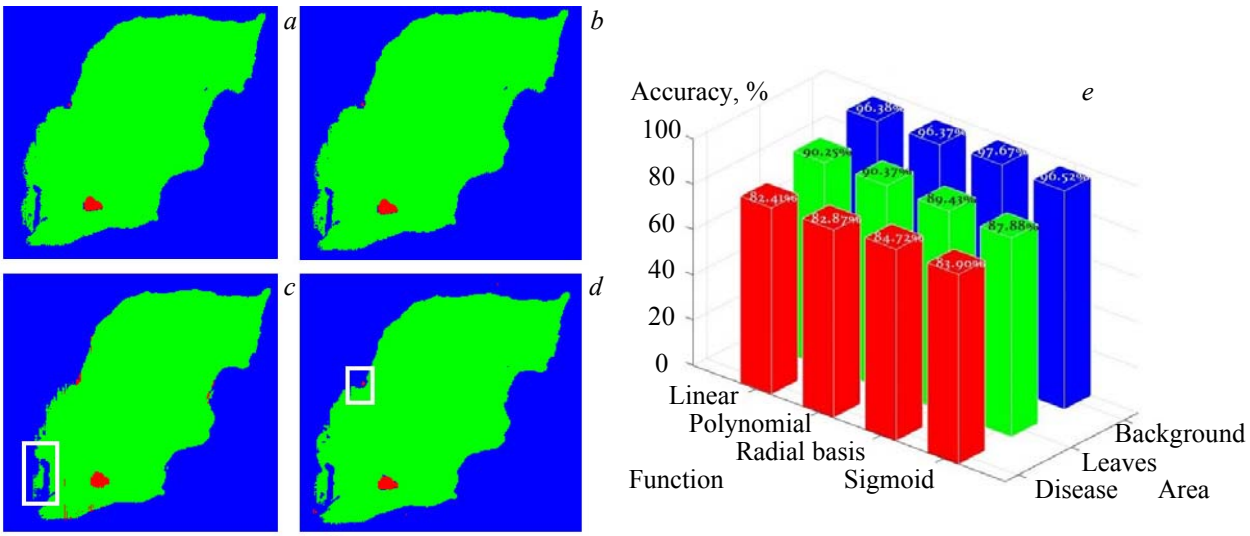

Fig. 6. Comparison of the support vector machine with different kernel functions: linear kernel (a), polynomial kernel (b), radial basis kernel (c), and sigmoid kernel (d) after dimensionality reduction, and (e) accuracy of the bar chart between different areas under different kernel functions.

To evaluate the SVM model, we use overall classification accuracy, kappa coefficient, and misclassification error to evaluate the recognition accuracy. The results of these two evaluation indicators are shown in Tables 1 and 2. We conclude that the accuracy of various kernel functions is generally around 94%. Among them, the radial basis function has the best effect, reaching 94.72%.

TABLE 1. Classification Accuracy of Various Kernel Functions and Kappa Coefficient

Function	Accuracy, %	Kappa coefficient
Radial basis fun	94.72	0.8839
Linear kernel	94.18	0.8726
Polynomial kernel	94.22	0.8733
Sigmoid kernel	93.37	0.8557

TABLE 2. Misclassification Error (%)

Class	Radial basis fun	Linear kernel	Polynomial kernel	Sigmoid kernel
Leaves	9.08	9.75	9.20	9.9
Disease	17.68	18.28	18.08	19.42
Background	3.4	3.62	3.33	3.5

Tables 1 and 2 show that the accuracy rate is totally above 93% in most cases, and the misclassification error rate is less than 15%. All four types of kernel functions obtain satisfactory results, which reflects the prospects of our n-SMT algorithm. Another evaluation method is the ROC curve, using the classification result to generate the ROC curve. This is shown in Fig. 7. The meaning of the area under a ROC curve corresponds to the probability of correct identification. We calculated the relative value below the ROC curve in Fig. 7, up to 84.5%. It reflects the satisfying effect of the combination of the n-SMT algorithm dimensionality reduction and the SVM classification.

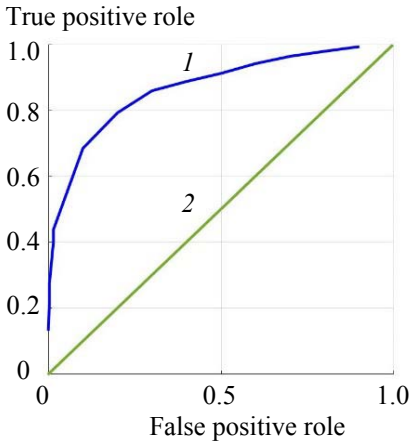

Fig. 7. Receiver-operating characteristic curve of the classification result:
1 – ROC curve, 2 – reference line with relative value of 50%.

Conclusions. We adopt the SMT model based on the maximum likelihood covariance estimation. We added the non-negative matrix to the SMT and optimized it to the n-SMT. We applied the n-SMT on a leaves dataset and performed dimensionality reduction on them. The result is super satisfactory. Also, we used another reduction algorithm on the same image and got two different results between the n-SMT result. Both of the algorithms can greatly achieve their purpose. The operating time of the n-SMT is less than for the MNF, and the accuracy is also extremely high. We can conclude that the n-SMT algorithm has advantages and can be effectively used for hyperspectral image dimension reduction.

REFERENCES

1. X. Jia, B. C. Kuo, M. M. Crawford, *Proc. IEEE,* **101**, No. 3, 676–697 (2013).
2. D. Landgrebe, *IEEE Signal Proc. Magazine*, **19**, No. 1, 17–28 (2002).
3. W. Jing, C. I. Chang, *IEEE Trans. Geosci. Remote*, **44**, No. 6, 1586–1600 (2006).
4. M. Fauvel, Y. Tarabalka, J. A. Benediktsson, J. Chanussot, J. Tilton, *Proc. IEEE*, **101**, No. 3, 652–675 (2013).
5. C. A. Manogue, T. Dray, *Mod. Phys. Lett. A*, **14**, No. 2, 99–103 (2013).
6. D. Zhang, Y. Le Y, *Int. Conf. Comput. Intelligence & Industrial Application* (2010).
7. L. R. Bachega, C. A. Bouman, *Int. Conf. Image Proc*. *IEEE* (2010).
8. A. L. Bertozzi, A. Flenner, *Multiscale Model Sim.*, **10**, No. 3, 1090–1118 (2012).
9. J. Theiler, G. Cao, et al., *IEEE J. Sel. Top. Signal Process*, **5**, No. 3, 424–437 (2011).
10. G. Cao, L. Bachega, et al., *IEEE Trans. Image Process*, **20**, No. 3, 625–640 (2011).
11. N. Kochan, G. Y. Tütüncü, G. Giner, *Expert Syst. Appl*., **167**, No. 3, 114200 (2020).
12. J. Fan, L. Yuan, *An. Stat*., **39**, No. 6, 3320–3356 (2011).
13. D. D. Lee, H. S. Seung, et al., *Nature*, **401**, 788–791 (1999).
14. P. O. Hoyer *J Mach. Learn Res*., **5**, No. 9, 1457–1469 (2004).
15. A. Copar, M. Zitnik, B. Zupan, *Biodata Min*., **10**, No. 1, 41 (2017).
16. Y. L. Xie, P. K. Hopke, P. Paatero, *J. Chem*., **12**, No. 6, 357–364 (2015).
17. H. Zhi, X. Yu, G. Wang, Z. Wang, *Fifth Int. Conf. Fuzzy System and Knowledge Discovery, FKSD 2008*, IEEE, **4**, 10–20, Jinan, Shandong, China (2008)
18. D. Bo, M. M. Lin, M. T. Chu, *Numer. Algorithms*, **65**, No. 2, 251–274 (2014).
19. Y. Chen, A. Wiesel, A. O. I. Hero, *IEEE Trans. Signal Process*, **59**, No. 9, 4097–4107 (2011).
20. M. Pal, G. Foody, *IEEE Trans. Geosci. Remote*, **48**, No. 5, 2297–2307 (2010).
21. Z. Emre, E. Tülin, M. E. Karslgil, *13th European Signal Processing Conference IEEE* (2015).
22. Y. Bazi, F. Melgani, *IEEE Trans. Geosci. Remote*, **44**, No. 11, 3374–3385 (2003).
23. K. Hajian-Tilaki, *Caspian J. Int. Med.*, **4**, No. 2, 627–635 (2013).
24. S. D. Walter, *State Med*., **24**, No. 13, 2025–2040 (2005).